Communication / Preliminary communication

2D *J*-resolved spiral spectroscopic imaging in rat brain at 7 T

Bassem Hiba, Anne Ziegler *

Laboratoire mixte Inserm/université Joseph-Fourier U594 'Neuroimagerie fonctionnelle et métabolique', laboratoire de recherche conventionné (30V) du CEA, Centre hospitalier universitaire, CHU pavillon B, BP 217, 38043 Grenoble cedex 9, France

Abstract

In order to decrease the total duration of 2D *J*-resolved 2D spectroscopic imaging, a fast spatial encoding by spiral trajectories was developed and added to a 2D *J*-resolved pulse sequence. Data were acquired on a rat brain in vivo at 7 T. Total acquisition time was about 42 min for a voxel size of 27 µl. A signal-to-noise ratio of 16.3 was measured on the NAA peak, enabling the reconstruction of metabolite maps for the main peaks. ***To cite this article: B. Hiba, A. Ziegler, C. R. Chimie 7 (2004).***
© 2004 Académie des sciences. Published by Elsevier SAS. All rights reserved.

Résumé

Pour diminuer les temps d'acquisition de données de spectroscopie 2D *J*-résolue localisées par imagerie spectroscopique in vivo, nous avons développé une séquence d'acquisition rapide par codage spiral de l'espace *k*. Cette méthode a été appliquée à l'acquisition de données sur le cerveau du rat à 7 T. Pour des voxels de 27 µl, le temps d'acquisition a été de 42 min, contre plus de 4 h par codage classique. Un rapport signal/bruit de 16,3 permet de reconstruire les images métaboliques des principaux pics.
Pour citer cet article : B. Hiba, A. Ziegler, C. R. Chimie 7 (2004).
© 2004 Académie des sciences. Published by Elsevier SAS. All rights reserved.

1. Introduction

Combining spectral and spatial information, Magnetic Resonance Spectroscopic Imaging (MRSI) provides distribution maps of metabolites. In standard experiments, the spatial information is obtained through phase encoding, requiring the acquisition of a number of scans at least equal to the number of voxels in the spectroscopic image. The spectral information is obtained through spin-echo or FID acquisition. In ^{1}H MRS, due to the high number of metabolites that can be detected in the brain, the narrow spectral range (around 10 ppm) of their resonances, the multiplet structure of *J*-coupled resonances, and the line broadening caused by the inhomogeneities of the local B_0 field, the peaks overlap, making quantification for mapping difficult.

Use of two-dimensional *J*-resolved spectroscopy is one way to avoid the peak overlap that 1D MRS suffers from. In 2D *J*-resolved spectra, the spectral information is spread onto a map: the chemical shift is encoded in the t_2 direction and the *J* coupling in the t_1 direction. It has been shown that 2D spectroscopic information can be combined with spatial encoding [1]. However, to obtain 2D spectroscopic images with high 2D spatial resolution, the acquisition time becomes excessive. For example, with a repetition time of 1 s, 32 encoding steps in both spatial directions, and 40 time increments, the minimum acquisition duration is longer than 11 h (without accumulation): this long duration strongly limits the biomedical use of such 4D techniques.

The minimum acquisition time of 4D SI can be reduced by using fast SI techniques based on various fast imaging solutions, including U-FLARE [2], echo-planar [3], multi-coil array [4] and spiral imaging [5]. Among these methods developed to reduce the minimum number of scans, the echo-planar SI based methods, for instance the Spiral Spectroscopic Imaging (SSI), use the delay between two successive time-domain points to sample spatial information. In SSI, the minimum acquisition time is reduced by applying a series of readout gradients during the acquisition window to collect simultaneously spatial and chemical shift information. Thanks to fast spiral encoding of the 2D spatial domain, the acquisition of t_1 data can be achieved in a reasonable time. On the other hand, a good quality of the gradient hardware, a gridding algorithm and the measurement of the actual *k*-space trajectory become necessary to obtain a spectroscopic image.

We propose a *k*-space trajectory waveform based on continuous series of growing and shrinking ('out-and-in') spirals [6] instead of just growing spirals, as are usually used in SSI [7]. Adding to the advantages of spiral imaging, like symmetry of *k*-space apodization by transverse relaxation effects, symmetry of gradient hardware demands, etc., out-and-in spiral *k*-space trajectories increase the robustness of SSI against the artefacts of flow and motion thanks to its readout gradient moment nulling, and also avoid specific rewinding gradients to return to the centre of *k*-space.

We present a high-spatial-resolution 4D out-and-in SSI experiment performed on rat brain at 7 T, and the data processing necessary to reconstruct the spiral

spectroscopic images. The quality of the image is evaluated by spatial-resolution estimation, and signal-to-noise measurement.

2. Method

2.1. Spiral spectroscopic imaging pulse sequence

During the rising (falling) part of each out-and-in spiral module, N_{rot} rotations are accomplished at constant angular velocity $\beta = 4 \pi N_{rot}/T$. The spiral radius increases or decreases linearly with time between 0 and k_{max}, at rate $\alpha = k_{max}/T$ [8]. A single rotation takes $T/(2 N_{rot})$ second, and the radius changes by k_{max}/N_{rot} at each turn. Using complex notation, the *k*-space trajectory curve $(k(t) = k_x(t) + i\ k_y(t))$ is described for a single out-and-in spiral module of duration *T* by:

$$k(t) = i\ \alpha\ t\ \exp[-i\ (\beta\ t + 2\ \pi\ s/N_k)]\ \text{for}\ 0 \le t < T/2$$

and

$$k(t) = i\ \alpha\ (T-t)\ \exp\left[i\ (\beta\ (T-t) - 2\ \pi\ s/N_k) \right]\ \text{for}\ T/2 \le t < T \quad (1)$$

A circular *k*-space region of diameter $2\ k_{max}$ is covered (Fig. 1). Segmentation in *k*-space is achieved by the initial phase term $2\ \pi\ s/N_k$, where $s = 0, \ldots$
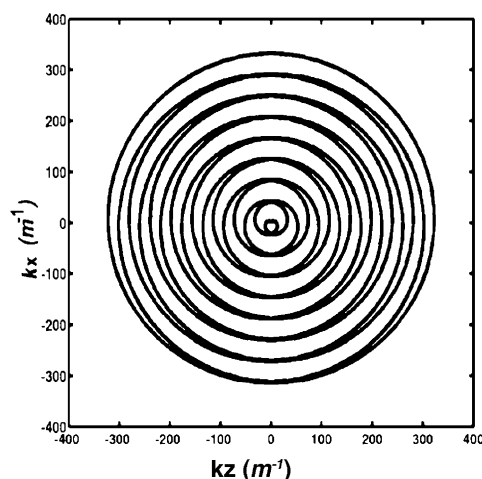

Fig. 1. Description of *k*-space by one single out-and-in spiral module of $N_{rot} = 8$ turns. Each *k*-space interleaf starts at the centre, goes out to the boundaries, and then returns to the centre of the *k*-space.
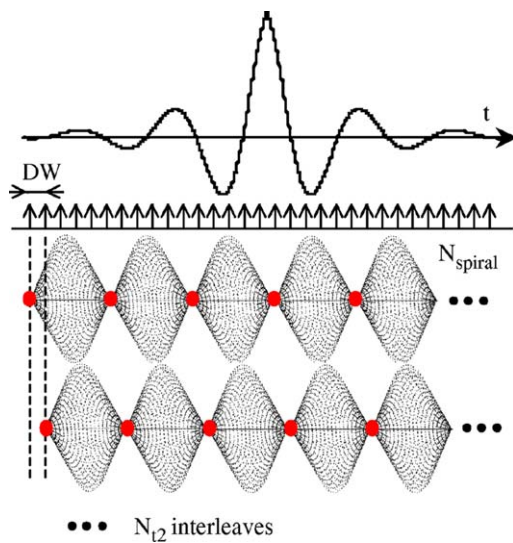
Fig. 2. The complete echo signal was sampled during application of spiral readout gradients (= 1024 points acquired for each spiral). To ensure correct spectral sampling, temporal interleaves were used by shifting the beginning of the acquisition window by DW. For each temporal interleaf, N_{spiral} samples (red points) were acquired to describe the t_2-dimension.
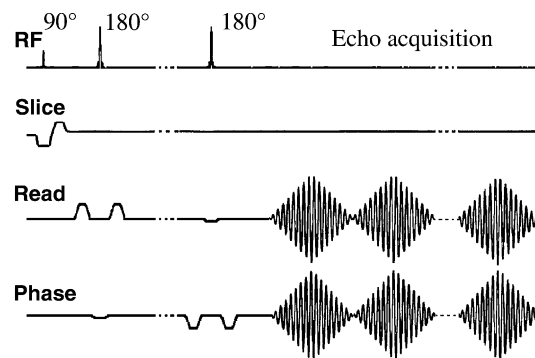

Fig. 3. The spiral spectroscopic imaging sequence consists in a PRESS module followed by out-in spiral readout gradients (water suppression and outer-volume saturation modules not shown). The t_1 domain was sampled by incrementing the echo time. The 180 slice-selective pulses were flanked by crusher gradients on read and phase channels.

N_k–1 is varied between acquisitions of the N_k k-space interleaves [9]. N_{dat} points were acquired during each spiral module.

In the t_2 domain, to sample the information over a spectral bandwidth *SW* (inverse of the sampling time *DW*), a single spiral should start every *DW*. At high field, to cover the 10-ppm bandwidth (^{1}H MRS spectral width), *DW* is shorter than at low field. Depending on the hardware limitations for gradient rise-time, it may be not possible to sample all the data associated with a particular k-space plane within such a short *DW*, so temporal interleaves may be required. N_{spiral} out-and-in spiral modules were applied after each excitation, and N_{t2} temporal interleaves were acquired by delaying by *DW* the opening of the acquisition window and, therefore, the start of the spiral readout gradients (Fig. 2). A total of $N = N_{t2} N_k N_{spiral} N_{dat}$ points were thus sampled during $N_{t2} N_k$ excitations that encoded the k_x, k_y, and t_2 domains. To describe the t_1 domain, N_{t1} increments were achieved by echo-time incrementation, leading to a total experiment time of $N_{t2} N_k N_{t1}$ *TR* N_a where *TR* is the repetition time and N_a the number of averages. More details can be found in [6].

Before the out-and-in spiral readout gradients, the volume of interest (VOI) was selected with a PRESS (Point-Resolved Spectroscopy) sequence [10] (Fig. 3). The PRESS sequence was preceded by a CHESS (Chemical Shift Selective) module for water suppression [11] and an outer-volume-saturation (OVS) module to decrease spatial contaminations.

2.2. Experiment and acquisition parameters

Experiments were performed on a SMIS console interfaced to a 7 T, 20-cm-diameter bore magnet (Magnex Scientific Ltd, Abingdon, UK), equipped with actively shielded Magnex gradients (MkSGRAD II, 200 mT m^{-1} max, 120 mm diameter) driven by gradient amplifiers Techron series 7700, with a maximum slew rate of 2 T m^{-1} ms^{-1}. MR data were collected from rat brain using a homemade single-turn surface coil (diameter 25 mm) for RF pulse transmission and signal reception.

All procedures involving animals conformed to the guidelines of the French Government (decree N°87-848 of 19 October 1987, licenses 006683 and A38071). Male Wistar rats (about 225 g) were used and anaesthesia was induced with 4% isoflurane in air (v/v) and then maintained with a mixture of 0.7–1.2% isoflurane in air enriched with oxygen to 30%. Rectal temperature was maintained at 36.5–37.5 °C by a regulated heating pad placed under the abdomen.

After obtaining scout-proton spin-echo images in transverse and coronal orientations, the PRESS VOI ($15 \times 18 \times 3$ mm^3) was localized in a slice parallel to the coil (*X, Z* horizontal plane). The field of view was

set to 30×30 mm^2. After manual shimming in the VOI (about 25 Hz FWHM for the water signal), the OVS and CHESS parameters were adjusted. During an acquisition window of 81.92 ms, 8192 data points were collected applying $N_{spiral} = 8$ out-and-in spiral readout gradient modules after each excitation. k-space covering of 2 $k_{max} = 666$ m^{-1} in both k_x and k_z directions leads to a nominal spatial resolution of 1.5 mm. Using 2 k-space interleaves ($N_k = 2$) and $N_{rot} = 8$ rotations, the FOV was 48 mm, computed from the sampling interval on the k-space axes (32 points sampled on each axis). To achieve a f_2 spectral bandwidth of 3125 Hz, $N_{t2} = 32$ temporal interleaves were acquired by incrementing the duration between the last RF pulse of the PRESS sequence and the opening of the acquisition window by $DW = 320$ μs. Starting at an echo time of 100 ms, 16 increments of 30 ms were performed in the t_1 domain resulting in a f_1 bandwidth of 33.33 Hz. To encode the k_x, k_z, and t_2 domains, an acquisition time of 2 min 40 s was required leading to a total acquisition time of 42 min 40 s (TR of 2500 ms).

2.3. SSI data processing

The k-space and the t_2 domain were partially sampled after each excitation. Therefore, (k_x, k_z, t_2) data of each t_1 step were first re-ordered into $\{(N_{spiral}+1) N_{t2} - 1\}$ time intervals of DW. Within each interval, samples were thus acquired for times t_i where:

$$i\,DW \leq t_i < (i + 1)\,DW, \text{ where } i = 0 \dots (N_{spiral} + 1) N_{t2} - 2 \quad (2)$$

For each (k_x, k_z) coordinate, a first-order phase correction was applied in the spectral domain to obtain the projection of the (k_x, k_z, t_i) data onto (k_x, k_z, $i\,DW$) planes. This will result in $\{(N_{spiral}+1) N_{t2} - 1\}$ (k_x, k_z) planes regularly spaced in the time direction.

The N_{t2} first and ($N_{t2} - 1$) last temporal planes of each t_1 step were rejected, resulting in a total of $\{(N_{spiral} - 1) N_{t2}\}$ (k_x, k_z) planes in the t_2 direction. This rejection was necessary because, in these first and last planes, the spiral had sampled only the centre of k-space, from one single point for the very first plane to an almost but not completely sampled k-space for the N_{t2}th one. Therefore, this insufficient sampling of k-space was likely to introduce some artefacts, and the corresponding planes were suppressed from the reconstruction.

In k-space, a gridding algorithm is needed for re-sampling the data of each temporal plane onto a Cartesian grid [12,13]. This was done as follows: (1) data were re-ordered according to spatial and spectral interleaving schemes; (2) FFT was done in the temporal domain followed by first-order phase correction in the spectral domain, and inverse FFT; (3) the temporal planes with insufficient sampling were rejected; (4) the spatial data were resampled onto a Cartesian grid with a Kaiser-Bessel interpolation kernel; (5) Hanning filtering and zero-filling points along both k-space axes, and 2D inverse FFT; the points outside the displayed FOV (30 mm) were discarded; (6) Hanning filtering, zero-filling and FFT in the t_2 domain; (7) Hanning filtering, zero-filling and FFT in the t_1 domain. All processing steps were performed with an in-house program in C. The metabolite images were computed by numerical integration of metabolite peaks all over the datasets.

The Kaiser–Bessel interpolation function used in the gridding step was computed with a window width $L = 3$ pixels of the Cartesian grid in both directions, and a half bandwidth product $B = \pi L$. The inverse of the sampling density compensation function necessary for the gridding algorithm [13] was calculated from the areas of the Voronoi diagram zones of the measured k-space trajectory.

3. Results

Digital resolutions of 6.1 Hz and 2.0 Hz per point were achieved in the f_2 and f_1 domains respectively. The resonances of N-acetylaspartate (NAA) at 2.0 ppm, glutamate/glutamine (Glu) at 2.4 ppm, creatine (Cre) at 3.0 ppm and choline (Cho) at 3.2 ppm were clearly observed on a 2D spectrum extracted from SSI datasets (Fig. 4). Fig. 5 shows the Cr (3.0 ppm) image computed from spiral spectroscopic datasets.

To evaluate the actual spatial resolution of the spectroscopic image, the theoretical point-spread function (PSF) was computed as a function of k-space sampling, gridding and spatial filtering (Fig. 6). The voxel size of the spectroscopic experiment was estimated to be 27.0 μl by numerical integration of the volume of the PSF function scaled to slice thickness.

The SNR was calculated from the intensity of the phased NAA peak divided by the noise r.m.s. measured
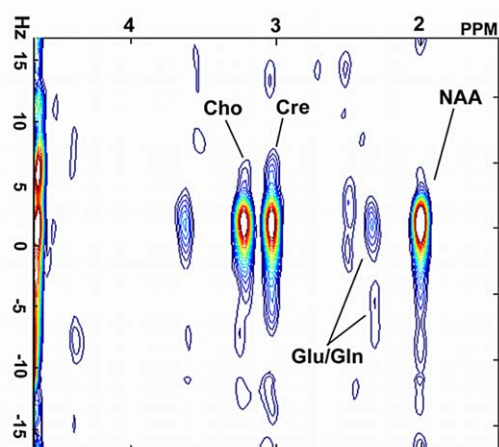
Fig. 4. A 2D *J*-resolved spectrum extracted from a SSI dataset on rat brain.
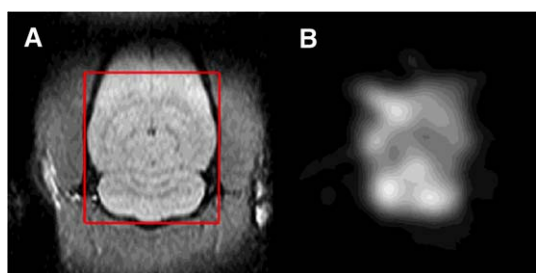

Fig. 5. (**A**) Proton spin-echo image corresponding to the slice in which the 4D dataset was acquired, with the contour (red box) of the volume-of-interest. (**B**) Metabolic image of Cr (3.0 ppm) from a rat brain in vivo from the 2D *J*-resolved 2D spatial dataset.
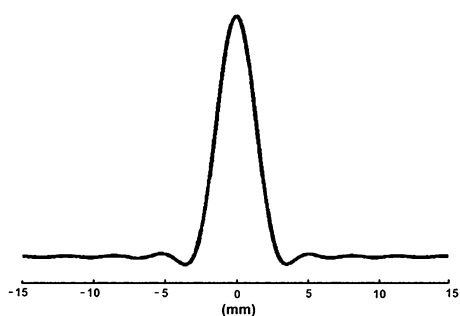

Fig. 6. Theoretical point-spread function corresponding to the sampling and processing used for the out-and-in spiral spectroscopic image (one axis): the volume under the 2D PSF gives the volume of the voxel (27 μl).

between 6 and 8 ppm. For 10 pixels spaced by more than the PSF FWHM (3 mm) of the SSI dataset, the average SNR was 16.3 ± 4.6.

4. Discussion

An in-vivo 2D *J*-resolved spiral spectroscopic image with 16 steps in t_1 and a 20×20 spatial matrix was achieved with a SNR higher than 16, in 42 min 40 s against 4 h 26 min for a standard phase encoding MRSI. The dependence of the PSF function on T_2^*, or on the chemical shift was not taken into account in the theoretical calculation, so the actual voxel size can be slightly larger than the 27 μl estimated from the SSI PSF.

The in-vivo high-resolution out-and-in SSI method combines high strength spiral readout gradients (up to 87.3 mT m^{-1}) and rapid commutations (up to 0.83 T m^{-1} ms^{-1}). This probably leads to a significant deviation between the theoretical and the actual *k*-space trajectories due to eddy currents, gradient system limits and pre-emphasis settings. To avoid all artefacts caused by this deviation, the actual *k*-space trajectory measured according to [14] was used to reconstruct the spectroscopic image.

Three-dimensional gridding was avoided by considering that the time-domain was regularly sampled throughout the data acquisition. First-order phase correction was used for data interpolation within a spectral dwell-time: gridding can be a time-consuming process, and our approach may be an advantageous alternative.

The *k*-space oversampling, resulting in a FOV of 48 mm, prevents the replica sidelobes produced by the gridding algorithm from being folded into the image of interest, and reduces the aliasing artefacts from the acquisition truncature. After the inverse FFT in the spatial domain, the data points outside of the FOV of interest were discarded, and only the data corresponding to a FOV of 30 mm containing the rat brain were kept and processed further.

Compared with standard spiral encoding, out-and-in spiral encoding somewhat increases the time efficiency of the sequence since all the data points collected in the acquisition window are used for image reconstruction. Moreover, thanks to the time symmetry of the gradient waveform, leading to periodically null gradient moments, the sensitivity to motion is further reduced, as recently demonstrated by Kim et al. [15].

5. Conclusion

We have demonstrated the feasibility of fast spiral 2D-spectral 2D-spatial spectroscopic imaging at high field in vivo. Mono-voxel clinical 2D spectroscopy has recently been proved useful for obtaining more information for spectral characterization and to better assign the resonances [16–18]. Robust rapid spectroscopic imaging techniques open the way to clinical applications of 2D spectroscopy.

Acknowledgements

References

[1]   M. von Kienlin, A. Ziegler, Y. Le Fur, C. Rubin, M. Décorps, C. Rémy, Magn. Reson. Med. 43 (2000) 211.

[2]   D. Mayer, W. Dreher, D. Leibfritz, Magn. Reson. Med. 49 (2003) 810.

[3]   D. Mayer, W. Dreher, D. Leibfritz, Magn. Reson. Med. 44 (2000) 23.

[4]   U. Dydak, M. Weiger, K.P. Pruessmann, D. Meier, P. Boesiger, Magn. Reson. Med. 46 (2001) 713.

[5]   E. Adalsteinsson, D.M. Spielman, Magn. Reson. Med. 41 (1999) 8.

[6]   B. Hiba, B. Faure, L. Lamalle, M. Décorps, A. Ziegler, Magn. Reson. Med. 50 (2003) 1127.

[7]   E. Adalsteinsson, P. Irarrazabal, D.M. Spielman, A. Macovski, Magn. Reson. Med. 33 (1995) 461.

[8]   C. Ahn, J. Kim, Z. Cho, IEEE Trans. Med. Imaging MI-5 (1986) 2.

[9]   C.H. Meyer, B.S. Hu, D.G. Nishimura, A. Macovski, Magn. Reson. Med. 28 (1992) 202.

[10] P.A. Bottomley, Ann. N. Y. Acad. Sci. 508 (1987) 333.

[11] A. Haase, J. Frahm, W. Hänicke, D. Matthaei, Phys. Med. Biol. 30 (1985) 341.

[12] H. Schomberg, J. Timmer, IEEE Trans. Med. Imaging 14 (1995) 596.

[13] V. Rasche, R. Proksa, R. Sinkus, P. Börnert, H. Eggers, IEEE Trans. Med. Imaging 18 (1999) 385.

[14] M.T. Alley, G.H. Glover, N.J. Pelc, Magn. Reson. Med. 39 (1998) 581.

[15] D.H. Kim, E. Adalsteinsson, D.M. Spielman, Magn. Reson. Med. 51 (2004) 458.

[16] M.A. Thomas, N. Binesh, K. Yue, N. DeBruhl, Magn. Reson. Imaging 14 (2001) 181.

[17] M.A. Thomas, K. Yue, N. Binesh, P. Davanzo, A. Kumar, B. Siegel, M. Frye, J. Curran, R. Lufkin, P. Martin, B. Guze, Magn. Reson. Med. 46 (2001) 58.

[18] A. Ziegler, B. Gillet, J.-C. Beloeil, J.-P. Macher, M. Décorps, J.-F. Nédelec, MAGMA 14 (2002) 45.